Arabian Journal of Chemistry (2023) **16**, 104991

King Saud University

Arabian Journal of Chemistry

www.ksu.edu.sa
www.sciencedirect.com

ORIGINAL ARTICLE

Discovery of novel 3-(piperazin-1-yl)propan-2-ol decorated carbazole derivatives as new membrane-targeting antibacterial agents

Ying-Guo Ding, Ai-Qun Chen, Na Wang, Zhou-Qing Long, Hong-Wu Liu, Jiao Xie, Shi-Tao Liu, Pu-Ying Qi, Xiang Zhou *, Li-Wei Liu, Song Yang *

National Key Laboratory of Green Pesticide, Key Laboratory of Green Pesticide and Agricultural Bioengineering, Ministry of Education, Center for R&D of Fine Chemicals of Guizhou University, Guiyang 550025, China

Received 10 February 2023; accepted 9 May 2023
Available online 18 May 2023

KEYWORDS

Carbazole derivatives;
Cell membrane;
Toxicity;
Microbial diseases;
Drug discovery

Abstract The increasing resistance problems of pathogens have drastically reduced the efficiency of existing drugs and agricultural chemicals, increasing the difficulty of preventing and controlling bacterial diseases. To create effective bactericide alternatives, a series of novel 3-(piperazin-1-yl) propan-2-ol decorated carbazole derivatives was fabricated, and their bioactivities and drug-likeness properties were evaluated. The *in vitro* bioassays showed that target molecules had outstanding antibacterial activity against *Xanthomonas oryzae* pv. *oryzae* (*Xoo*), *Xanthomonas axonopodis* pv. *citri* (*Xac*), and *Pseudomonas syringae* pv. *actinidiae* (*Psa*), with optimal EC_{50} values of 6.80 μg/mL (**A_9**), 6.37 μg/mL (**A_9**), and 10.75 μg/mL (**A_{10}**), respectively. Furthermore, a series of biochemical assays indicated that title molecules could negatively impact the function of bacteria by irreversibly damaging their cell membranes, resulting in cytoplasmic components leakage (nucleic acids and proteins). In addition, phytotoxicity test and *in silico* toxicity predictions suggested that compound **A_9** had low phytotoxicity, and possessed acceptable drug-like properties. Our results showed that carbazole derivatives containing an 3-(piperazin-1-yl)propan-2-ol moiety were promising skeletons to develop novel bactericides with low toxicity for controlling refractory microbial diseases by targeting cell membranes.

* Corresponding authors.
E-mail addresses: xiangzhou@gzu.edu.cn (X. Zhou), syang@gzu.edu.cn (S. Yang).

Peer review under responsibility of King Saud University.

Production and hosting by Elsevier

https://doi.org/10.1016/j.arabjc.2023.104991

1. Introduction

Plant bacterial diseases are posed by numerous phytopathogenic bacteria, which are difficult to control, and cause an irretrievable loss of agricultural production globally (Ali et al., 2022; Zeng et al., 2022). Some intractable phytopathogenic bacteria, such as *Xanthomonas oryzae* pv. *oryzae* (*Xoo*) (Sciallano et al., 2022; Zheng et al., 2021; Yang et al., 2021), *Xanthomonas axonopodis* pv. *citri* (*Xac*) (Zhu et al., 2022; Gao et al., 2017), and *Pseudomonas syringae* pv. *actinidiae* (*Psa*) (Tahir et al., 2020; Liu et al., 2022), are quite problematic for growers and can invade a variety of crops such as rice, citrus, and kiwi fruit (Moon et al., 2022; Nayem et al., 2020; Wicaksono et al., 2018). The use of chemical bactericides is currently still the most effective way to manage these diseases. Unfortunately, the existing bactericides [bismerthiazol (BT), and thiodiazole copper (TC)] possess a reduced control efficiency duo to emerging an increased bacterial resistance caused by long-term use of pesticides (Li et al., 2018; Song et al., 2022; Liu et al., 2022a, 2022b). Even worse, the use of large doses of traditional pesticides leads to environmental pollution and adversely affects human health (Zhou et al., 2022a, 2022b). Therefore, it is necessary to excavate new green pesticides with high efficiency and low toxicity. Notably, targeting membrane agents have become an attractive strategy for treating pathogenic microorganisms due to breaking the bacterial cell membrane, and killing the bacteria, thereby restricting the resistance risk (Côté et al., 2019; Cai et al., 2022).

Natural products, as a source of inspiration for pesticides, have attracted much attention due to their diverse structure, abundance of resources, and low negative effect on the environment (Zhou et al., 2022a, 2022b; Pereira, et al., 2022; Al-Yousef et al., 2021; Zang et al., 2020; Thawabteh et al., 2019). In particular, as displayed in Fig. 1, carbazole alkaloids are a crucial structural motif that is prevalent in the natural world, and many naturally and structurally modified carbazole derivatives possess extensive biological activity (Cheng et al., 2021), including antibacterial (Salih et al., 2016), antifungal (Nalli et al., 2016), antitumor (Fu et al., 2021), antioxidative (Bandgar et al., 2012), anti-inflammatory activity (Pattanashetty et al., 2018). Some carbazole alkaloids, such as ellipticine (Grau et al., 2020), carvedilol (Zhu et al., 2013), and carprofen (Parra et al., 2016), have been used in disease prevention in humans. In our previous work, carbazole derivatives containing isopropanolamine or 1, 2, 3-triazole fragments proved to be potential antimicrobial agents with obviously negative effects on the cell membrane (Zhao et al., 2019; Huang et al., 2021). Therefore, carbazoles represent a promising skeleton for use in new drugs and pesticides.

In an effort to extend the potential of carbazoles, we found that some molecules possessed outstanding antimicrobial activity *via* targeting the cell membrane (Lin et al., 2020; Xue et al., 2021; Zhang et al., 2010). Thus, carbazoles could be regarded as a template for the fabrication and development of membrane-targeting agents (Hurley et al., 2015). More interestingly, some compounds containing piperazine (Casalone et al., 2022; Prasad et al., 2022) and amide (Feng et al., 2022a, 2022b) scaffolds also possess remarkable antimicrobial activity *via* targeting the cell membrane, such as an ((phenyl)sulfonyl)piperazine derivative (Prasad et al., 2022) and compound Ac12 (Chen et al., 2021). Therefore, rational molecular design might lead to the development of new membrane-targeting agents.

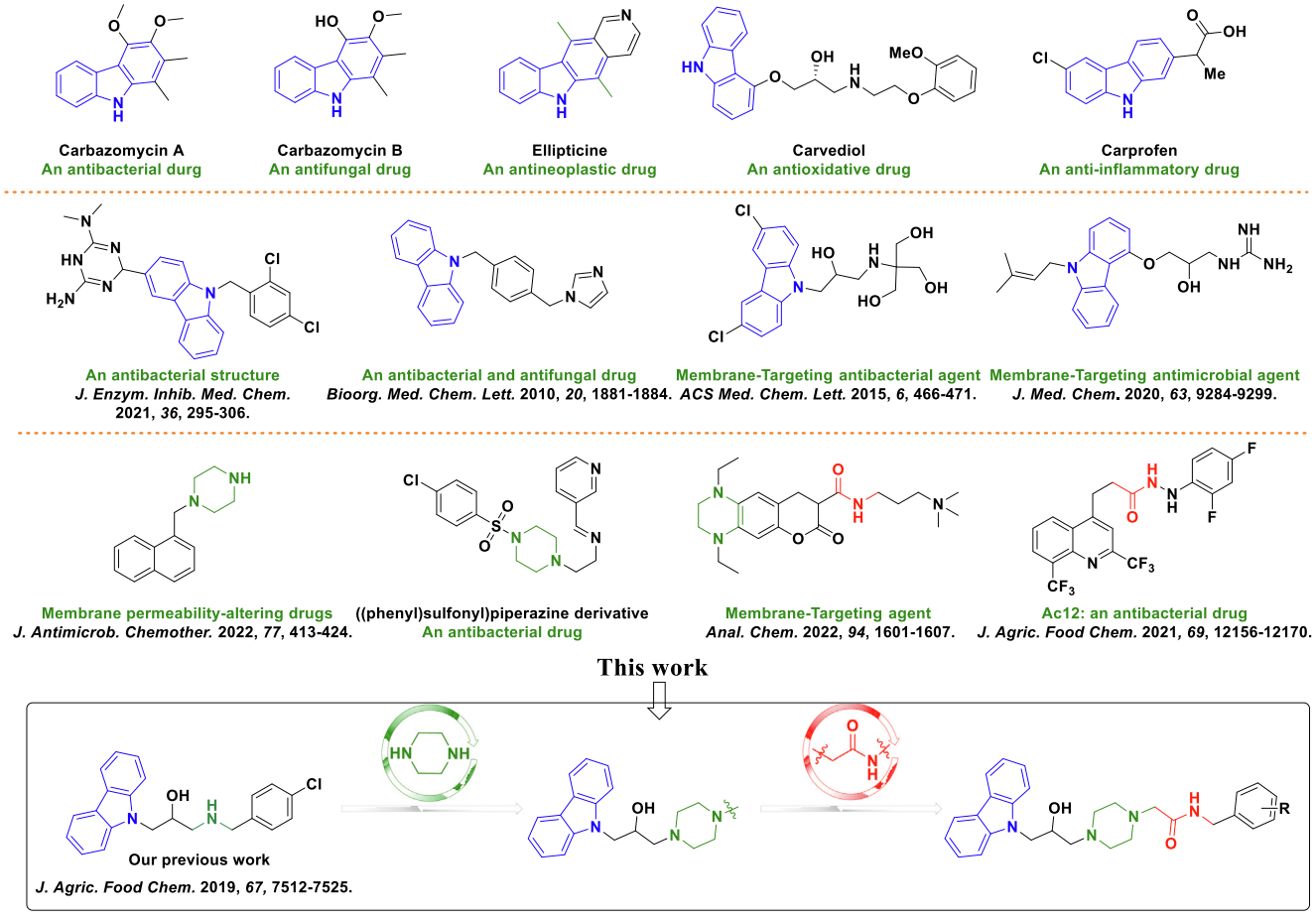

Fig. 1 Some bioactive structures containing carbazole, piperazine, and amide moieties and the design strategy for target molecules.

Herein, to explore more effective membrane-targeting agents, a series of novel 3-(piperazin-1-yl)propan-2-ol decorated carbazole derivatives were designed and synthesized *via* a molecular hybridization strategy. Furthermore, the antimicrobial behavior of the title molecule was investigated by various biochemical assays. To verify the toxic active of title molecules, we also investigated the phytotoxicity and *in silico* 'drug-likeness' of the synthetic compounds.

2. Materials and methods

2.1. Instruments and chemicals

NMR spectra were recorded on a JEOL–ECX 500 (500 MHz, JEOL Ltd., Tokyo, Japan) or Bruker Biospin AG-400 instrument (400 MHz, Bruker Optics, Switzerland). High-resolution mass spectrometry (HRMS) data was performed with a Q-Exactive Orbitrap MS apparatus (Thermo Fisher Scientific, USA). Scanning electron microscopy (SEM) images were obtained by a Nova NanoSEM 450 (FEI, USA). Fluorescent images were obtained by an Olympus BX53 microscope (Tokyo, Japan). Optical density (OD) was recorded on a Cytation™ 5 multi-mode reader (BioTek Instruments, Inc., USA). Cell membrane permeability assay was measured using a DDS-307 electrical conductivity analyzer. All chemicals and solvents were purchased from commercial sources.

2.2. Experimental section

The antibacterial activity *in vitro* and *in vivo*, morphological study, growth curve, and the cell membrane permeability assay were conducted *via* previously reported methods (Feng et al., 2022a, 2022b; Wang et al., 2022).

2.3. Propidium iodide (PI) staining experiment for Xoo cells

To further observe the damage to the bacteria cell membrane (Gan et al. 2020), the active compound **A9** (anti-*Xoo*, EC_{50} = 6.80 μg/mL) was chosen to carry out a PI staining assay. Briefly, *Xoo* cells at logarithmic phase (OD_{595} = 0.6–0.8) were collected *via* centrifugation (8000 rpm, 2 min, 4 °C), and resuspended with phosphate buffer saline (PBS, 10 mM, pH = 7.2) to an OD_{595} value of 0.1. Then, 1 mL of the resuspended *Xoo* cells was incubated with compound **A9** at various concentrations (6.8, 13.6, and 27.2 μg/mL) in a shaker (28 °C, 180 rpm) for 14 h. The same volume of DMSO was used as a negative control. After that, 100 μL of the treated *Xoo* cultures was incubated with 10 μL of PI dye solution (20 μg/mL) for 20 min. Finally, fluorescence images of the treated *Xoo* cells were collected.

2.4. Bioassay of intracellular substance leakage

The leakage of nucleic acid and protein in *Xoo* cells was determined according to a previously reported method (Xiang et al., 2018; Cockrell et al., 2015), and the active compound **A9** (anti-*Xoo*, EC_{50} = 6.80 μg/mL) was chosen as the treatment agent. Briefly, *Xoo* cells at logarithmic phase (OD_{595} = 0.6–0.8) were collected *via* centrifugation (8000 rpm, 2 min, 4 °C), and resuspended in PBS buffer to an OD_{595} value of 0.1. Then, 1 mL of the resuspended *Xoo* cells (OD_{595} = 0.1) was incubated with different dosages of compound **A9** in a shaker for 14 h. After that, the supernatants of the samples were collected *via* centrifugation (8000 rpm, 2 min, 4 °C). Finally, the content of nucleic acid and protein in the supernatants was immediately detected using an ultra-micro spectrophotometer instrument (NanoPhotometer N50).

2.5. Fourier-transform infrared spectroscopy (FTIR)

FTIR was applied to intensively investigate the interaction between bacterial cell membrane and title compounds (Cockrell et al., 2015; Poonprasartporn and Chan, 2021). Briefly, after undergoing the same treatment as the experiment in Section 2.3, 13.6 μg/mL of compound **A9** and equivoluminal DMSO were incubated with *Xoo* bacterial suspension (OD_{595} = 0.1) in a shaker (28 °C, 180 rpm) for 14 h. The bacterial suspension was then harvested by centrifugation (8000 rpm, 2 min, 4 °C), and then re-suspended by PBS. Samples were dried and then stored in the freeze dryer for backup.

All FTIR spectra were recorded by the Nicolet iS50 FT-IR spectrophotometer in transmission mode, and the FTIR data were obtained in the wavelength range of 4000–400 cm^{-1}.

2.6. Effect of compound A9 on extracellular polymeric substances (EPS)

The effect of molecule **A9** on the EPS production of *Xoo* cells was assayed *via* our previously reported method (DuBois et al., 2002; Qi et al., 2022). Briefly, 0.1 (OD_{595}) of *Xoo* cells was incubated with compound **A9** at final dosages of 1.7, 3.4, 6.8, and 13.6 μg/mL in a shaker for 3 d. Finally, the relative production of EPS in different samples was measured according to the xanthan gum standard curve. Each assay was repeated at three times independently.

2.7. Scanning electron microscopy analysis

A morphological study of the *Xoo* cells was assayed referring to previous works (Feng et al., 2022a, 2022b; Wang et al., 2023). Briefly, 15 mL of *Xoo* cells (OD_{595} = 0.2) was transferred to sterile 50 mL centrifuge tubes. After incubating with different dosages (0, 6.8, 13.6, 27.2, and 54.4 μg/mL) of compound **A9** in a shaker for 14 h, the *Xoo* cells were gently washed with PBS, fixed with 2.5 % glutaraldehyde, and gradually dehydrated with different concentration of ethanol. Finally, the samples were freeze-dried, gold-sprayed, and captured by SEM.

2.8. The phytotoxicity and in silico pharmacokinetics prediction

Firstly, in ChemDraw (version Ultra 14.0, PerkinElmer Informatics, Waltham, MA, USA), the structure of molecule **A9** was transformed into their SMILES format. Drug-likeness predictions were then conducted using ADMETlab 2.0 (https://admetmesh.scbdd.com) accessed on 26 Oct. 2022.

2.9. Statistical analysis

All experiments were carried out at least in triplicate. Growth curves and extracellular substance leakage results were processed using Origin 2021 software. Statistical analyses were

executed using one-way ANOVA in the SPSS 20.0 software. The bioassay results were reported as the mean ± SD.

3. Results and discussion

3.1. Chemistry

A facile synthetic route for 3-(piperazin-1-yl)propan-2-ol decorated carbazole derivatives was proposed. First, 9*H*-carbazole was firstly reacted with epibromohydrin to generate intermediate **1**. Second, intermediate **1** was ring-opened with 1-boc piperazine, and then intermediate **2** bearing a piperazine group was obtained through removal of the boc group. (The more detail synthesis route could be found in **Figure S1-S2**). The target compounds $\mathbf{A_1}$–$\mathbf{A_{13}}$ were finally obtained by nucleophilic substitution reaction of intermediate **2** with intermediate **3** (Fig. 2**&Figure S3**). Similarly, the target compounds $\mathbf{A_{14}}$–$\mathbf{A_{18}}$ were synthesized *via* a ring-opening reaction between intermediate **1** and different 1-substituted piperazines (Fig. 3), the general procedure for the preparation of the compounds $\mathbf{A_{19}}$ and $\mathbf{A_{20}}$ could be found in **Figure S4**).

All of the title molecules were verified by ^{1}H NMR, ^{13}C NMR, ^{19}F NMR and HRMS. For instance, in ^{1}H NMR spectra, three double peaks (d) occurred in the range of δ 8.08–8.13, 7.62–7.65 and 7.47–7.39 ppm, and the triplet peak (t) displayed at δ 7.16–7.20 ppm, which belonged to protons of the carbazole ring. The double peak (d) located in δ 8.09–8.36 ppm was signed as the characteristic peak of N–H ($\mathbf{A_1}$–$\mathbf{A_{13}}$). Other peaks located in δ 7.04–7.60 ppm were attributed to the phenyl group. The doublet of doublets peaks (dd) at δ 4.46–4.54 ppm and 4.26–4.33 ppm was generated by the methylene group which connected between isopropanol and carbazole moiety. The single peak (s) between 4.01 ppm and 4.28 ppm was the CH_2-CH-CH_2 moiety. The peaks in the range of δ 2.93–3.04 ppm and δ 3.36–3.55 ppm were the characteristic of the piperazine-CH_2 of compounds $\mathbf{A_1}$–$\mathbf{A_{13}}$ and $\mathbf{A_{15}}$–$\mathbf{A_{18}}$. The protons of alkyl linker (isopropanol-CH_2-piperazine) could be identified at δ 2.50–2.60 ppm. Multiple peaks at δ 2.30–2.55 ppm were the signals of the piperazine moiety. For compounds $\mathbf{A_1}$–$\mathbf{A_{13}}$, the single peak (s) at δ 4.22–4.40 ppm was singed as the benzyl-CH_2. Moreover, in the ^{13}C NMR spectra, the characteristic peaks of the carbazole moiety were signaled at δ 141.02–141.21, 125.96–125.77, 122.53–122.45, 120.30–120.55 and 119.06–119.27 ppm, respectively. Notably, a strong peak at δ 169.43–170.34 ppm was the characteristic peak of the carbonyl group of compounds $\mathbf{A_1}$–$\mathbf{A_{13}}$ and $\mathbf{A_{19}}$. Other signals at δ 159.25–113.78 represented the characteristic peaks of phenyl group. The signals of the piperazine moiety were observed at δ 52.74–53.90 and 47.90–48.14 ppm, and the characteristic peaks of isopropanol moiety were validated at δ 67.80–67.41, 62.43–62.08 and 59.78–53.84 ppm. Specially, split peaks at δ 160.46–162.66, 129.24–130.63, 123.61–124.75 and 114.28–115.50 ppm belonged to the carbon of phenyl-F for compounds $\mathbf{A_4}$–$\mathbf{A_6}$, respectively. In addition, in ^{19}F NMR spectra, the phenyl-F for compounds $\mathbf{A_4}$–$\mathbf{A_6}$ and the CF_3 signals of compounds $\mathbf{A_{10}}$ mainly occurred at δ −119.17, −113.59, −116.28 and −60.76 ppm, respectively. Finally, for the all the synthesized target compounds, their exact molecular weight could be found in HR(ESI)MS spectra by comparing with the theoretical values. The above analysis indicated that the title compounds were successfully prepared, and detailed date could be found in the Supplementary Materials. (**Figure S5-68**).

3.2. Antibacterial activities and SAR analysis

A preliminary *in vitro* bioassay of the title compounds was performed with the turbidimeter test (Wang et al., 2023). The commercial bactericides TC and BT were used as positive controls. The bioassay outcomes (Table 1) revealed that most of the target compounds showed remarkable bactericidal activity against all the tested bacterial strains, affording EC_{50} values

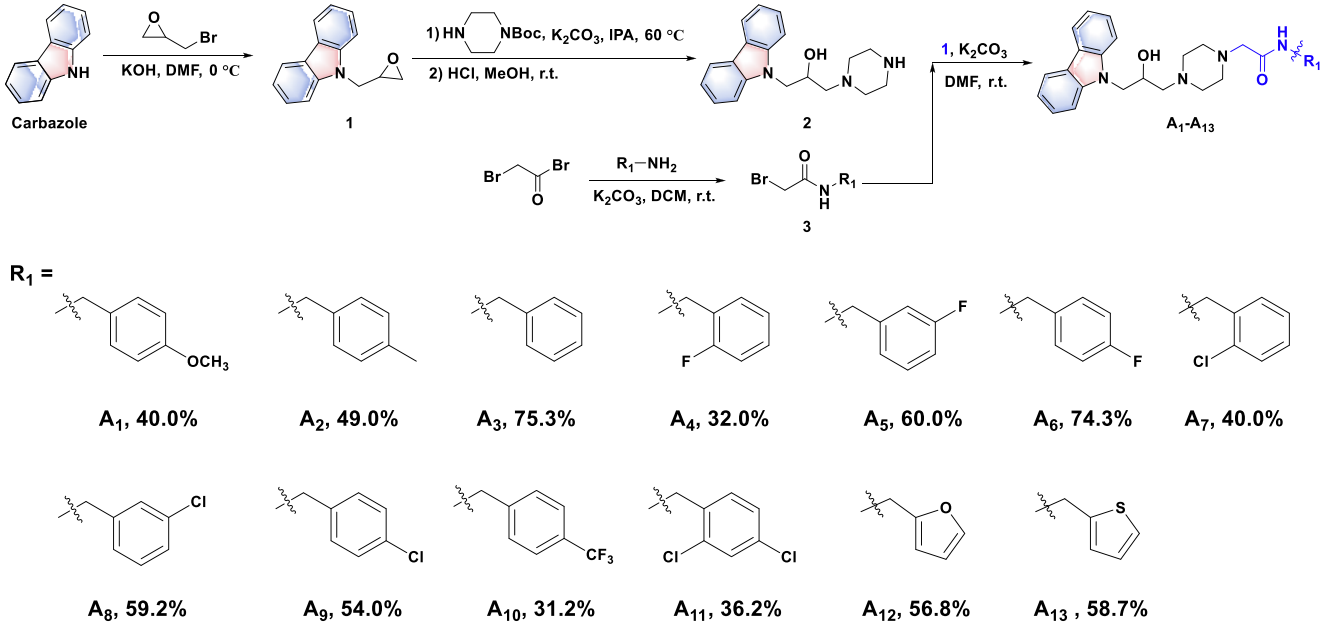

Fig. 2 Synthesis route for target molecules $\mathbf{A_1}$–$\mathbf{A_{13}}$.

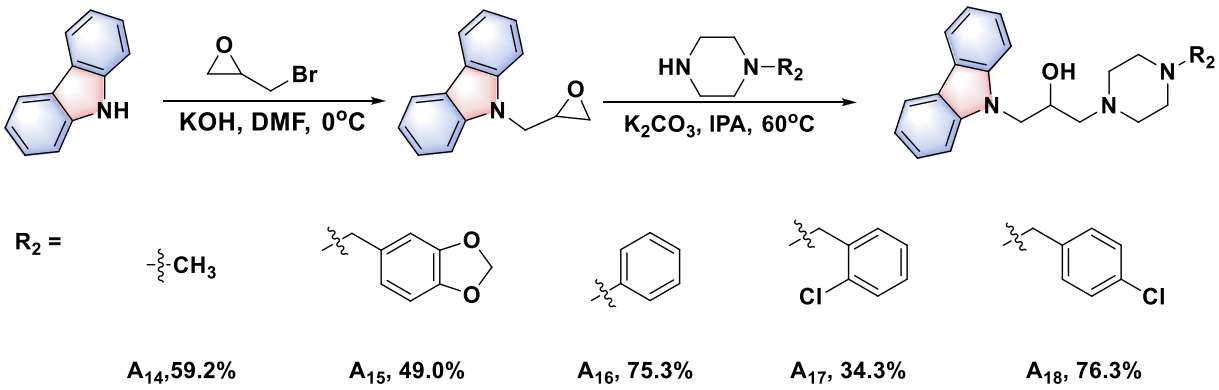

Fig. 3 Synthetic route for compounds $\mathbf{A_{14}}$–$\mathbf{A_{18}}$.

Table 1 *In vitro* bioactivities of compounds $\mathbf{A_1}$–$\mathbf{A_{13}}$ against pathogens *Xoo, Xac,* and *Psa*.

Compd.	*Xoo*		*Xac*		*Psa*	
	regression equation	EC_{50} (μg/mL)[a]	regression equation	EC_{50} (μg/mL)[a]	regression equation	EC_{50} (μg/mL)[a]
A_1	y = 5.5994x − 2.4072	20.03 ± 1.31	y = 5.3636x − 1.9743	19.97 ± 0.54	y = 2.6269x ± 1.4257	22.94 ± 0.48
A_2	y = 7.4634x − 1.5724	7.60 ± 0.12	y = 4.0136x + 0.8309	10.93 ± 1.00	y = 2.6722x + 0.6665	41.85 ± 2.23
A_3	y = 3.4381x + 1.7449	8.85 ± 0.30	y = 2.4192x + 2.6410	9.44 ± 0.24	y = 1.5671x + 2.9197	21.27 ± 1.55
A_4	y = 5.3659x − 1.9700	19.90 ± 0.78	y = 3.8595x + 0.1020	18.57 ± 0.99		> 100
A_5	y = 5.6853x − 2.4181	20.17 ± 0.75	y = 6.8270x + 2.5643	12.82 ± 0.55		> 100
A_6	y = 5.7575x − 1.0896	11.42 ± 0.07	y = 6.1388x − 1.4993	11.45 ± 0.20	y = 1.6058x + 3.0377	16.67 ± 1.52
A_7	y = 4.9967x + 0.2835	8.78 ± 0.10	y = 2.8562x + 2.4239	7.98 ± 0.35	y = 2.5163x + 0.5876	56.69 ± 8.64
A_8	y = 8.2138x − 3.2233	10.03 ± 0.17	y = 4.3883x + 1.0392	8.00 ± 0.68		>100
A_9	y = 11.207x − 4.3286	6.80 ± 0.16	y = 3.2233x + 2.4078	6.37 ± 0.52	y = 3.191x + 0.171	32.61 ± 5.81
A_{10}	y = 4.1642x − 1.4784	7.01 ± 0.44	y = 2.9768x + 2.3660	7.67 ± 0.40	y = 2.7091x + 2.2057	10.75 ± 0.68
A_{11}	y = 12.358x − 5.6733	7.31 ± 0.97	y = 4.8225x + 0.3799	9.08 ± 0.56		>100
A_{12}	y = 5.8677x + 4.6092	43.42 ± 2.18	y = 3.1705x + 0.3144	25.49 ± 2.79	y = 2.6061x + 0.0748	77.60 ± 2.02
A_{13}	y = 43.945x − 66.794	43.03 ± 1.61	y = 6.7760x − 4.0359	21.55 ± 2.27		>100
BT[b]	y = 9.8313x − 9.5823	30.43 ± 0.33	y = 3.5826x − 1.8056	79.36 ± 4.97		>100
TC[b]	y = 7.6119x − 9.5933	82.64 ± 2.57	y = 9.4833x − 12.045	62.71 ± 2.32		>100

[a] EC_{50} values of antibacterial potency were indicated as the mean ± SD (standard deviation) of three independent repetitions.
[b] Commercialized antibacterial agents as positive controls. Abbreviations: BT, bismerthiazol; TC, thiodiazole copper.

that were much lower than those of BT and TC. Especially, compound $\mathbf{A_9}$ proved to have the most potent antibacterial activity against *Xoo* and *Xac*, with EC_{50} values of 6.80 and 6.37 μg/mL, respectively. In addition, compounds $\mathbf{A_1}$, $\mathbf{A_2}$–$\mathbf{A_8}$, $\mathbf{A_{10}}$ and $\mathbf{A_{11}}$ displayed excellent anti-*Xoo* potency, with EC_{50} values ranging from 7.01 to 20.17 μg/mL. Moreover, compounds $\mathbf{A_3}$, $\mathbf{A_7}$, $\mathbf{A_8}$, $\mathbf{A_{10}}$, and $\mathbf{A_{11}}$ revealed excellent anti-*Xac* activity, with EC_{50} values of 9.44, 7.98, 8.00, 7.67 and 9.08 μg/mL, respectively, which were quite better than TC (62.71 μg/mL) and BT (79.36 μg/mL). Interestingly, compounds $\mathbf{A_{12}}$ and $\mathbf{A_{13}}$ had lower biological activity against *Xoo* than other compounds, with EC_{50} values of 43.42 μg/mL and 43.03 μg/mL. For anti-*Psa* activity, compared with the control agents BT (>100 μg/mL) and TC (>100 μg/mL), compounds $\mathbf{A_6}$ and $\mathbf{A_{10}}$ showed significant antibacterial activity, with EC_{50} values of 16.67 μg/mL and 10.75 μg/mL, respectively.

The structure–activity relationships analysis (SARs) of target compounds $\mathbf{A_1}$–$\mathbf{A_{13}}$ against *Xoo* were summarized as follows: 1) compared with compound $\mathbf{A_3}$, the introduction of electron-withdrawing groups on the benzene ring was commonly more beneficial to enhance antibacterial potency compared to electron-donating groups, such as compounds $\mathbf{A_9}$ (4-Cl, 6.80 μg/mL), $\mathbf{A_{10}}$ (4-CF_3, 7.01 μg/mL), $\mathbf{A_6}$ (4-F, 11.42 μg/mL), $\mathbf{A_3}$ (4-H-Ph, 8.85 μg/mL), and $\mathbf{A_1}$ (4-OCH_3-Ph, 20.03 μg/mL); 2) the positions of substituents on the benzene ring were generally affected the anti-*Xoo* ability, as the following order: $\mathbf{A_9}$ (4-Cl, 6.80 μg/mL) > $\mathbf{A_7}$ (2-Cl, 8.78 μg/mL) > $\mathbf{A_8}$ (3-Cl, 10.03 μg/mL), and $\mathbf{A_6}$ (4-F, 11.42 μg/mL) > $\mathbf{A_4}$ (2-F, 19.90 μg/mL) > $\mathbf{A_5}$ (3-F, 20.17 μg/mL); 3) the compounds that introduced a benzyl amine moiety were much better than those with a five-membered heterocyclic methylamine, namely, the activity of compounds $\mathbf{A_1}$–$\mathbf{A_{11}}$ was superior to that of compounds $\mathbf{A_{12}}$–$\mathbf{A_{13}}$. As for anti-*Xac* and anti-*Psa* activity, the similar trends were observed. All the analyses suggested that introducing a 4-electron-withdrawing substituted benzyl amine moiety to the 3-(piperazin-1-yl) propan-2-ol decorated carbazole derivatives could significantly enhance antibacterial potency. Especially, the 4-Cl-benzyl moiety-containing compound $\mathbf{A_9}$ afforded the most active EC_{50} values of 6.80 μg/mL and 6.37 μg/mL toward *Xoo* and *Xac*, respectively, and compound $\mathbf{A_{10}}$ (4-CF_3-benzyl) was the most active molecule of all the title compounds in terms of anti-*Psa* activity.

To study the effect of amide groups on antibacterial potency, a new series of 3-(piperazin-1-yl)propan-2-ol decorated carbazole derivatives (**A_{14}–A_{18}**) was designed and synthesized (Fig. 3), the compounds **A_{19}** and **A_{20}** could be found in **Figure S4**). The *in vitro* bioassays (Table 2) showed that the antibacterial potency of title molecules **A_{14}–A_{20}** was dramatically decreased after the amide group was removed, affording EC_{50} values of over 100 μg/mL toward all the tested phytopathogenic bacteria (*Xoo*, *Xac*, and *Psa*); except for compound **A_{15}**, which afforded a moderate EC_{50} value of 40.63 μg/mL against *Xoo*, and compound **A_{17}**, which afforded outstanding biological activity with EC_{50} values of 11.42 μg/mL against *Xoo* and 16.35 μg/mL against *Xac*. Furthermore, compared with compound **A_3**, compound **A_{16}** afforded EC_{50} values of over 100 μg/mL toward all the tested phytopathogenic bacteria (*Xoo*, *Xac*, and *Psa*). Similar results were found in other compounds, such as compounds **A_7**, **A_8** and **A_9**, affording the remarkable antibacterial activities than compounds **A_{17}** and **A_{18}**. However, when introducing benzoyl unit and (phenyl)sulfonyl unit to parent skeleton, the compounds **A_{19}** and **A_{20}** were inactive for fighting against three pathogenic bacteria. These results suggested that the amide groups of compounds **A_1–A_{14}** were key active cores for their excellent bactericidal competence.

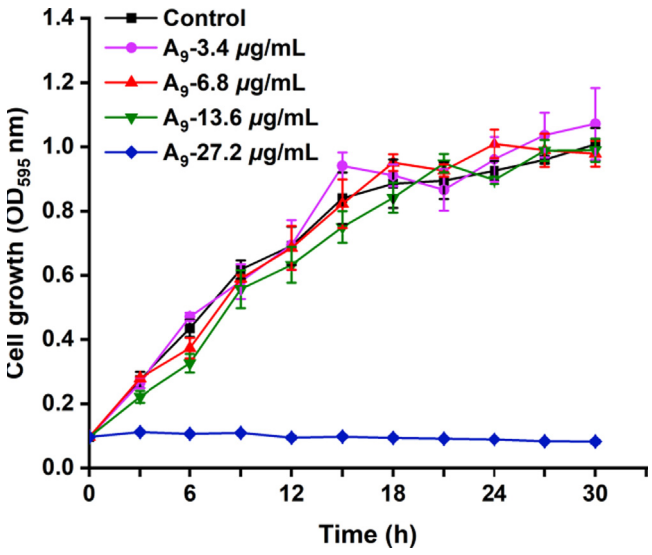

Fig. 5 Growth curve of *Xoo* treated with compound **A_9** at 0, 3.4, 6.8, 13.6, and 27.2 μg/mL.

Table 2 *In vitro* bioactivities of compounds **A_{14}–A_{20}** against pathogens *Xoo*, *Xac*, and *Psa*.

Compd.	*Xoo*		*Xac*		*Psa*	
	regression equation	EC_{50} (μg/mL)[a]	regression equation	EC_{50} (μg/mL)[a]	regression equation	EC_{50} (μg/mL)[a]
A_{14}	y = 5.6818x − 4.31718 4.3171	40.63 ± 1.65		> 100		> 100
A_{15}		> 100		> 100		> 100
A_{16}		> 100		> 100		> 100
A_{17}	y = 3.1182x + 1.7020	11.42 ± 1.59	y = 2.1058x + 2.4445	16.35 ± 1.35		> 100
A_{18}		> 100		> 100		> 100
A_{19}		> 100		> 100		> 100
A_{20}		> 100		> 100		> 100
BT[b]	y = 9.8313x − 9.5823	30.43 ± 0.33	y = 3.5826x − 1.8056	79.36 ± 4.97		> 100
TC[b]	y = 7.6119x − 9.5933	82.64 ± 2.57	y = 9.4833x − 12.045	62.71 ± 2.32		> 100

[a] EC_{50} values of antibacterial potency were indicated as the mean ± SD (standard deviation) of three independent repetitions.
[b] Commercialized antibacterial agents as positive controls. Abbreviations: BT, bismerthiazol; TC, thiodiazole copper.

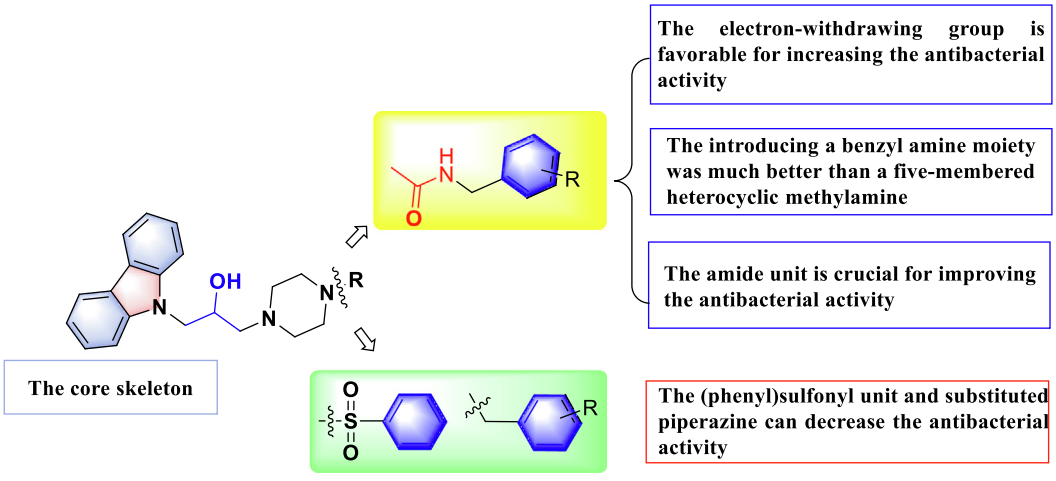

Fig. 4 Diagram of structure–activity relationship (SAR) analyses.

Finally, a detailed SAR analysis of the title molecules was depicted in Fig. 4.

3.3. Growth curves of *Xoo* cells triggered by compound A_9

Based on *in vitro* bactericidal bioassays, the most active compound **A_9**, was selected to investigate the antibacterial mechanism, and the growth curve test was used to evaluate the effect of compound **A_9** on *Xoo* (Qi et al., 2022; Zhou et al., 2021). As shown in Fig. 5, compared to the control group (0 μg/mL), cell growth was not obviously affected after treating with compound **A_9** at concentrations of 3.4, 6.8, and 13.6 μg/mL, respectively. However, significant change occurred when *Xoo* cells were incubated with compound **A_9** at 27.2 μg/mL. The

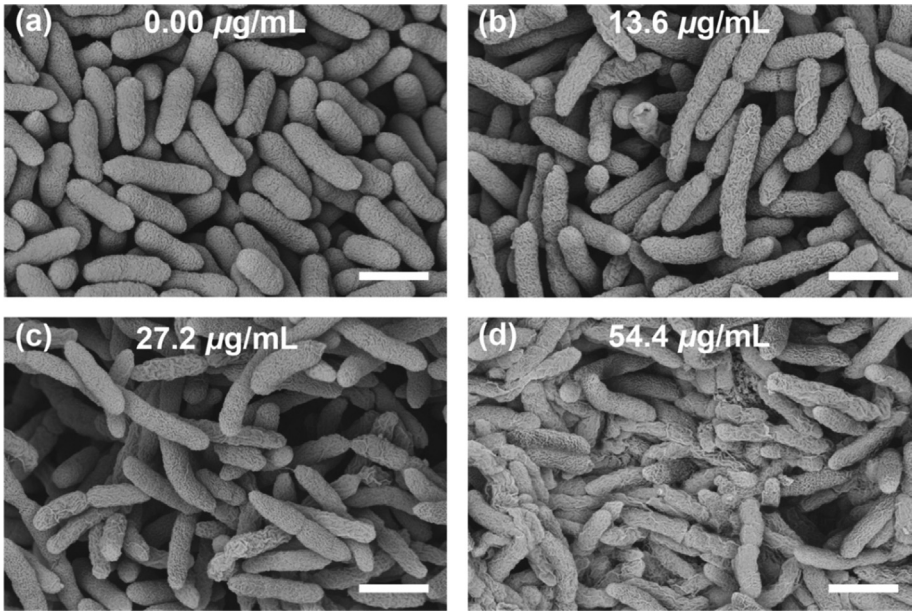

Fig. 6 Scanning electron microscopic results of *Xoo* cells after treating with compound **A_9** at (a) 0 μg/mL, (b) 13.6 μg/mL, (c) 27.2 μg/mL, and (d) 54.4 μg/mL. The scale bars represent 1 μm.

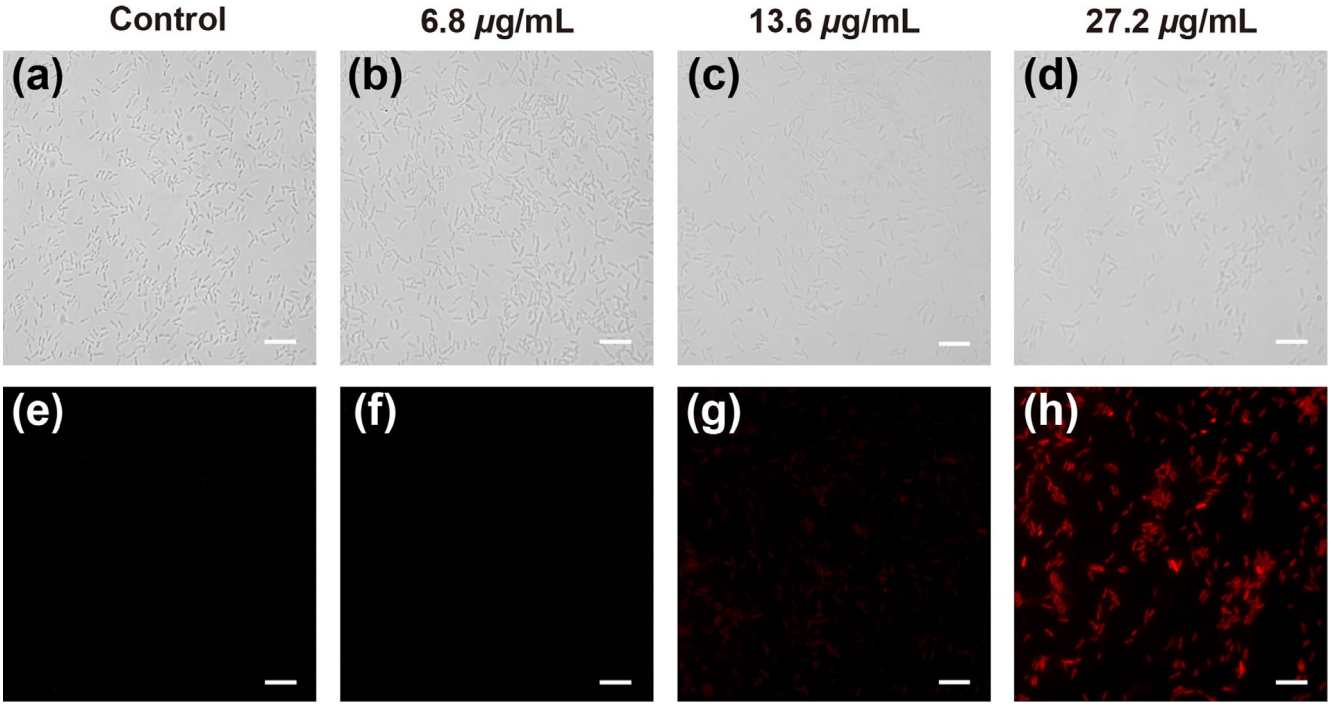

Fig. 7 Morphology of *Xoo* cells stained with PI after incubation with compound **A_9** at (a,e) 0 μg/mL, (b,f) 6.8 μg/mL, (c,g) 13.6 μg/mL, and (d,h) 27.2 μg/mL. The image a-d was obtained from regular observation and the image e-h was obtained from fluorescent observation for *Xoo* cells. The scale bars represent 10 μm.

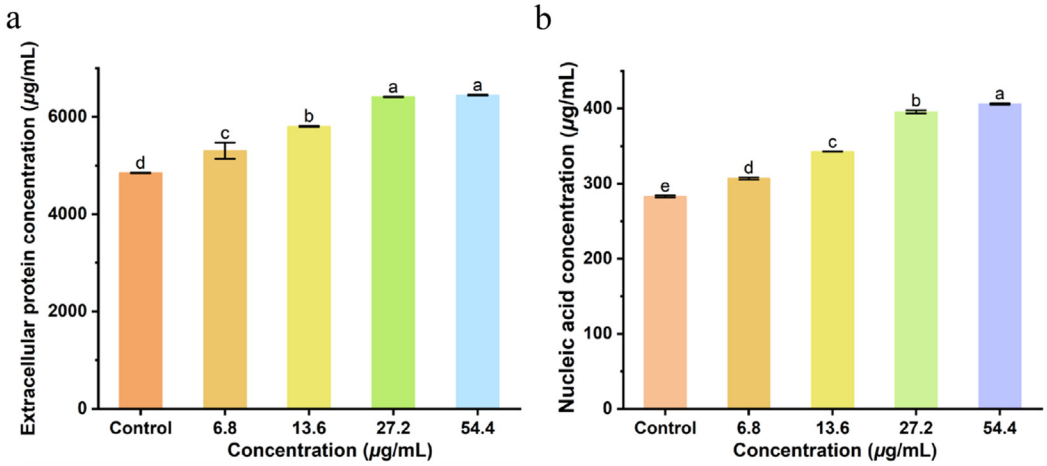

Fig. 8 The concentration of extracellular protein and nucleic of *Xoo* cells after incubation with various concentrations of **A9**: 0 μg/mL (CK), 1.7 μg/mL, 3.4 μg/mL, 6.8 μg/mL and 13.6 μg/mL.

results showed that compound **A9** could significantly affect the growth of phytopathogenic bacteria at concentrations being over 27.2 μg/mL.

3.4. Morphological study of Xoo cells

To study the morphological impact of the title compound on the tested bacteria, *Xoo* cells were treated with the active compound **A9** and then observed *via* SEM (Wang et al., 2022). As displayed in Fig. 6, the surface of the control *Xoo* was smooth and full. However, many damaged cells appeared after treating with compound **A9** at 13.6 μg/mL, and more cells were corrugated or even seriously malformed and cracked with increased concentration (Fig. 6c and 6d). These findings suggested that compound **A9** could negatively impact the physiological function and morphology of bacteria, which might be key factors for bacterial death.

3.5. PI staining experiment for Xoo cells

PI, an effective indicator dye, emits red fluorescence upon intercalating with DNA (Zhang et al., 2018), and the intensity can indirectly reflect the vitality and membrane permeability of cells. As shown in Fig. 7, the fluorescence intensity increased with an increase in the dosage of compound **A9**. Specifically, the sample treated by compound **A9** at 6.8 μg/mL showed weak red fluorescence intensity, which was comparative to that of blank controls (0 μg/mL, healthy cells). However, slight red fluorescence was observed at 13.6 μg/mL (Fig. 7g), and strong red fluorescence (Fig. 7h) was observed at 27.2 μg/mL, which suggested that the damage to the *Xoo* cell membrane increased with increasing dosage of compound **A9**. The results showed that cell membrane permeability could be negatively affected

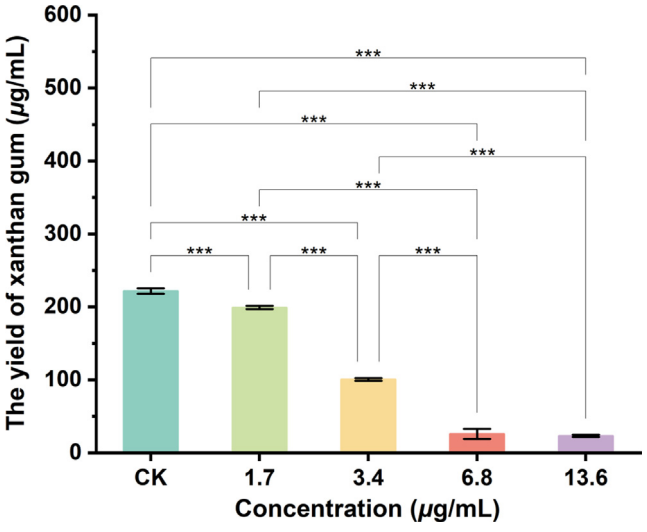

Fig. 9 Inhibition of the reduction of extracellular polysaccharide of *Xoo* cells in vivo protein content after 72 h incubation in various concentrations of **A9**, respectively. 0 μg/mL(CK), 1.7 μg/mL, 3.4 μg/mL, 6.8 μg/mL and 13.6 μg/mL. (*p < 0.05, **p < 0.01, ***p < 0.001).

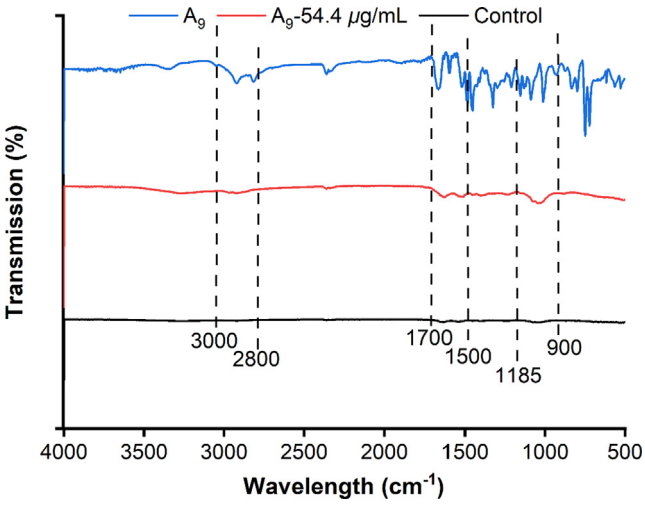

Fig. 10 FTIR spectra (500–4000 cm^{-1}) of *Xoo* cells after incubation with different concentrations (0 μg/mL, 6.8 μg/mL, and 13.6 μg/mL) of compound **A9**.

by compound **A9**, which was consistent with the SEM results and may be a key factor for causing cell death.

3.6. Compound A9 induced leakage of cellular nucleic acids and proteins

As an important indicator of cell membrane damage, the leakage of nucleic acids and proteins from *Xoo* cells was verified (Xiang et al., 2018; Ning et al., 2019). As shown in Fig. 8, the lowest extracellular protein content and nucleic acid leakage was seen in the control treatment at 4852.0 μg/mL and 280.1 μg/mL, respectively, which indicated that the cell wall and membrane was unbroken. However, a distinct increase in extracellular protein and nucleic acid content was observed after treating with compound **A9**, with the leakage amount being positively correlated with concentration, indicating that compound **A9** could cause evident damage to the integrity of *Xoo* and resulted in the leakage of intracellular nucleic acids, proteins, and other functional molecules.

3.7. Effects of compound A9 on extracellular polysaccharide production

Many studies had shown that EPS could not only enhance the resistance of bacteria to harsh environments, but it could also be considered a virulence factor in evading host defenses (Qi et al., 2022). In one study, xanthan gum, as one of the main components of EPS, was produced on cell membranes (Sutherland, 1982), which served as a key indicator of the viability of phytopathogenic *Xanthomonas* (Picchi et al., 2021). As shown in Fig. 9, the EPS yield of *Xoo* cells (199.16 μg/mL) treated with compound **A9** at 1.7 μg/mL was slightly lower than that of the control group (221.76 μg/mL) and displayed more significant decreases at elevated dosages. For example, the EPS yield decreased to 100.58 and 25.89 μg/mL when incubated with compound **A9** at 3.4 and 6.8 μg/mL, respectively.

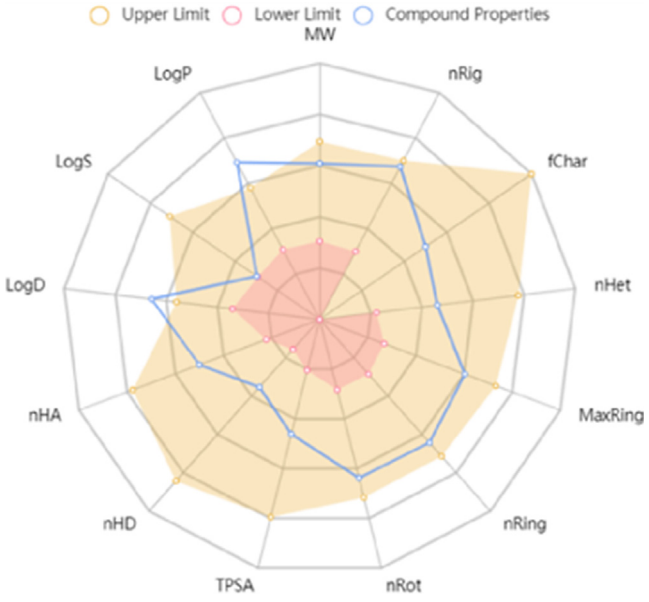

Fig. 12 Physicochemical properties of compound **A9**.

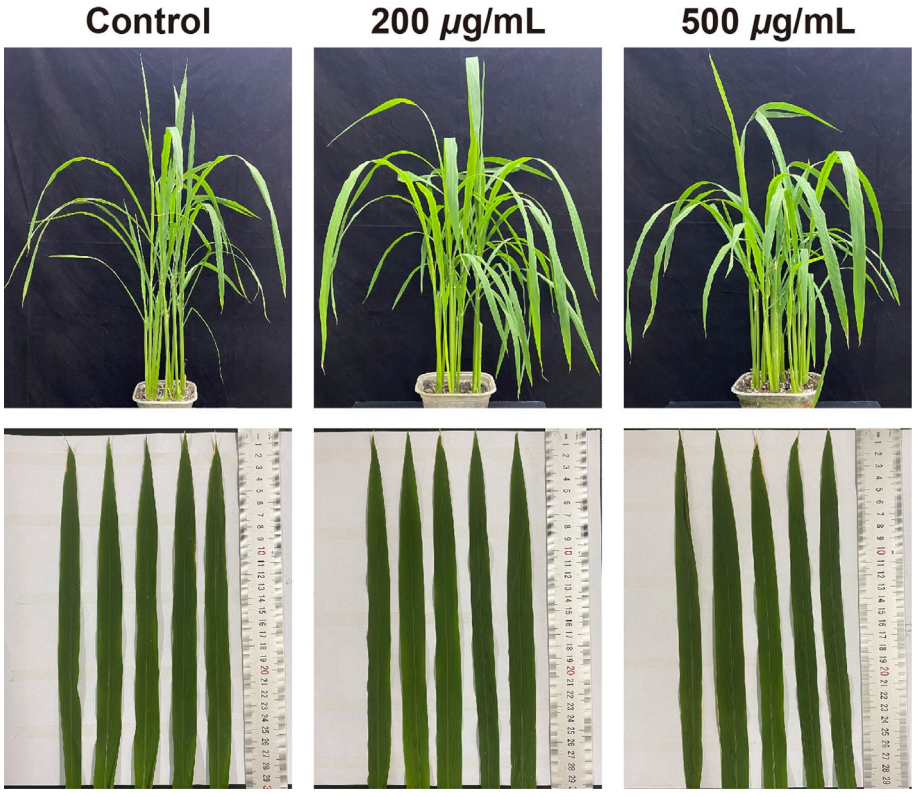

Fig. 11 The phytotoxicity of compound **A9**.

Our findings indicated that molecule **A9** could significantly suppress the production of EPS in phytopathogenic bacteria.

3.8. Fourier transform infrared spectroscopy

The IR bands of different biomolecular characteristics were investigated: lipids (3000–2800 cm^{-1}), protein/amides I and II (1700–1500 cm^{-1}), phospholipids/DNA/RNA (1500–1185 cm^{-1}), polysaccharides (1185–900 cm^{-1}), and the fingerprint region (900–600 cm^{-1}) (He et al., 2021). As shown in Fig. 10, the effects of compound **A9** and *Xoo*, individually and combined, on the bacterial membrane were analyzed *via* FT-IR. The outcomes reflected the changes of the molecular composition of *Xoo* bacteria before and after treating with compound **A9**. Upon treatment with 54.4 μg/mL of compound **A9** + *Xoo* cells, the peak intensity at 3000 cm^{-1} and 2800 cm^{-1} was slightly increased compared to the control group. And the evident change was found at 1185–900 cm^{-1}, which belonged to IR bands of polysaccharides. Meanwhile, the results were agreed with similar literature (Ojeda et al., 2008; Stenclova et al., 2019). Interestingly, compared with the control, an enhanced vibration peaks at 1500–1700 cm^{-1} was observed, which belonged to C—N stretching, C═O stretching, N—H bending and stretching, and protein/amides I and II. These outcomes were consistent with previous works (Zhou et al., 2021; Biswas et al., 2019). When the cell membrane was dis-

Table 3 ADMET and drug-like properties of compound **A9** *via* the online prediction tool ADMETlab 2.0.

	Property	Value	Decision
Absorption	Caco-2 Permeability	−5.433	Medium
	Madin–Darby canine kidney cells (MDCK) (Pgp) permeability (cm/s)	0.000015	Excellent
	Human intestinal absorption (HIA) (%)	0.103	Excellent
Distribution	Plasma protein binding (PPB)(%)	96.88	Bad
	Volume distribution (VD) (L/kg)	1.98	Excellent
	Excretion		
	Clearance (mL/min/kg)	10.526	Excellent
	The half-life ($T_{1/2}$) (h)	0.054	
Toxicity	Rat oral acute toxicity	0.723	Bad
	Skin sensitization	0.131	Excellent
	Eye corrosion	0.003	Excellent
	Eye irritation	0.007	Excellent
	Respiratory toxicity	0.845	Bad
Drug-likeness	Lipinski rule	Accepted	Excellent
	Golden triangle	Accepted	Excellent

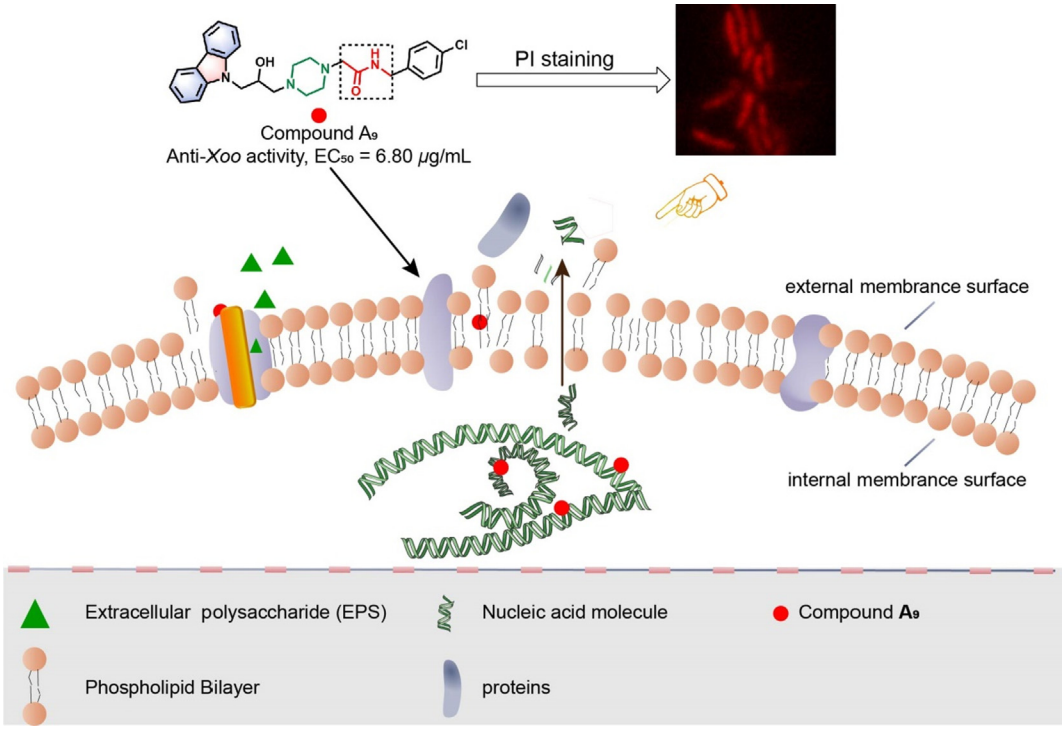

Fig. 13 The hypothesized mechanism of action of compound **A9**.

turbed, the corresponding absorption peak intensity increased significantly, reflecting cell damage and death. Indicating that compound **A9** could potentially change the *Xoo* cell membrane.

3.9. The phytotoxicity and in silico 'drug-likeness' evaluation of the title compound

Finally, the most important step for pharmaceutical development is assessing the potential of lead compounds in the early time (Zhou et al., 2022a, 2022b). Therefore, to evaluate whether molecule **A9** has potential as a lead compound, the toxic activity and pharmacokinetic information was obtained. For instance, the phytotoxicity was assayed by rice plant and displayed in Fig. 11, after 7 day incubation, compound **A9** exhibited non-toxicity toward rice (Zhou et al., 2021; Mukhtar et al., 2020). Furthermore, the ADMET and drug-like properties of compound **A9** were achieved by ADMETlab 2.0 software (Xiong et al., 2021). The physicochemical, ADMET, and drug-like properties of the selected molecule **A9** are shown in Fig. 12 and Table 3. Remarkably, compound **A9** exhibited reasonable physicochemical, ADMET, and pharmaceutical properties, with molecular weight = 490.21, logS = − 3.946, logP = 4.234, and logD = 3.883. Furthermore, the ADMET and drug-like properties of compound **A9** were determined: 1) it possessed definite absorption capacity with excellent activity in human intestinal absorption (HIA), and its permeability in Madin–Darby canine kidney cells (MDCK) (Pgp) was 1.5×10^{-5} cm/s; 2) it had a low VD value; 3) it was conventionally safe (*e.g.*, low skin sensitization, eye irritation, and eye corrosion); and 4) it had great potential drug-likeness properties, including the Lipinski rule and the golden triangle rule. In addition, the metabolism property of compound **A9** was provided in **Table S1**. In short, the above results indicated that compound **A9** had acceptable pharmacokinetic characteristics and low phytotoxicity, suggesting a promising antimicrobial selectivity.

4. Conclusion

In summary, a series of 3-(piperazin-1-yl)propan-2-ol decorated carbazole analogues was fabricated, and assessed for antibacterial potency. The *in vitro* bioassay indicated that most of the target molecules had remarkable bactericidal potency against malignant phytopathogenic bacteria, including *Xoo*, *Xac*, and *Psa*, with EC_{50} values of 6.80, 6.37, and 10.75 μg/mL, respectively, which were much better than those of commercial bactericides BT (30.43, 79.36 and > 100 μg/mL) and TC (82.64, 62.71, and > 100 μg/mL). Furthermore, the SAR analysis suggested that the electron-withdrawing substituted benzyl amine moiety and the amide groups of compounds **A_1–A_{14}** served as the key active core for their excellent bactericidal competence. Moreover, the SEM, PI staining, and cellular nucleic acids and proteins leakage experiments indicated that compound **A9** could negatively impact the physiological function and morphology of the bacteria cell membrane, change its permeability, and lead to the leakage of cellular nucleic acids and proteins, which may be the key factor for bacterial death. The corresponding action mechanism was displayed in Fig. 13. In addition, compound **A9** also could significantly inhibit the production of EPS in phytopathogenic bacteria, which indirectly explained the effect of compound **A9** on the bacteria cell membrane. Finally, phytotoxicity test exhibited that compound **A9** had low phytotoxicity, and *in silico* predictions suggested that compound **A9** possessed acceptable drug-like properties. Our results showed that compound **A9** could be regarded as a potential lead compound to develop novel membrane-targeting agents for treating pathogenic microorganisms' infection.

CRediT authorship contribution statement

Ying-Guo Ding: Investigation, Formal analysis, Methodology, Writing – original draft. **Ai-Qun Chen:** Investigation. **Na Wang:** Investigation, Formal analysis. **Zhou-Qing Long:** Investigation, Formal analysis. **Hong-Wu Liu:** Investigation, Formal analysis. **Jiao Xie:** Investigation. **Shi-Tao Liu:** Visualization. **Pu-Ying Qi:** Visualization. **Xiang Zhou:** Investigation, Funding acquisition, Writing – review & editing. **Li-Wei Liu:** Investigation, Formal analysis. **Song Yang:** Supervision, Funding acquisition, Project administration, Methodology, Writing – review & editing.

Declaration of Competing Interest

The authors declare that they have no known competing financial interests or personal relationships that could have appeared to influence the work reported in this paper.

Acknowledgements

We acknowledge the supports form National Key Research and Development Program of China (2022YFD1700300), National Natural Science Foundation of China (21877021, 32160661, 32202359), the Guizhou Provincial S&T Project (2018[4007]), the Guizhou Province [Qianjiaohe KY number (2020)004]), Program of Introducing Talents of Discipline to Universities of China (D20023, 111 Program), and GZU (Guizhou University) Found for Newly Enrolled Talent (No. 202229).

Appendix A. Supplementary material

Supplementary data to this article can be found online at https://doi.org/10.1016/j.arabjc.2023.104991.

References

Ali, Q., Zheng, H., Rao, M.J., Ali, M., Hussain, A., Saleem, M.H., Nehela, Y., Sohail, M.A., Ahmed, A.M., Kubar, K.A., Ali, S., Usman, K., Manghwar, H., Zhou, L., 2022. Advances, limitations, and prospects of biosensing technology for detecting phytopathogenic bacteria. Chemosphere 296,. https://doi.org/10.1016/j.chemosphere.2022.133773 133773.

Al-Yousef, H.M., Amina, M., 2021. Phytoconstituents and pharmacological activities of cyanobacterium *Fischerella ambigua*. Arab. J. Chem. 14, (6). https://doi.org/10.1016/j.arabjc.2021.103153 103153.

Bandgar, B.P., Adsul, L.K., Chavan, H.V., Jalde, S.S., Shringare, S. N., Shaikh, R., Meshram, R.J., Gacche, R.N., Masand, V., 2012. Synthesis, biological evaluation, and docking studies of 3-(substituted)-aryl-5-(9-methyl-3-carbazole)-1*H*-2-pyrazolines as potent anti-inflammatory and antioxidant agents. Bioorg. Med. Chem. Lett. 22 (18), 5839–5844. https://doi.org/10.1016/j.bmcl.2012.07.080.

Biswas, D., Tiwari, M., Tiwari, V., 2019. Molecular mechanism of antimicrobial activity of chlorhexidine against carbapenem-resistant *Acinetobacter baumannii*. PLoS One. 14 (10), e0224107.

Cai, Y.Y., Zou, G.M., Xi, M.H., Hou, Y.J., Shen, H.Y., Ao, J.F., Li, M., Wang, J., Luo, A.W., 2022. Juglone Inhibits *Listeria monocytogenes* ATCC 19115 by Targeting Cell Membrane and Protein. Foods 11 (17), 2558. https://doi.org/10.3390/foods11172558.

Casalone, E., Vignolini, T., Braconi, L., Gardini, L., Capitanio, M., Pavone, F.S., Giovannelli, L., Dei, S., Teodori, E., 2022. Characterization of substituted piperazines able to reverse MDR in *Escherichia coli* strains overexpressing resistance-nodulation-cell division (RND) efflux pumps. J. Antimicrob. Chemother. 77 (2), 413–424. https://doi.org/10.1093/jac/dkab388.

Chen, Y.J., Ma, K.Y., Du, S.S., Zhang, Z.J., Wu, T.L., Sun, Y., Liu, Y.Q., Yin, X.D., Zhou, R., Yan, Y.F., Wang, R.X., He, Y.H., Chu, Q.R., Tang, C., 2021. Antifungal Exploration of Quinoline Derivatives against Phytopathogenic Fungi Inspired by Quinine Alkaloids. J. Agric. Food Chem. 69 (41), 12156–12170. https://doi.org/10.1021/acs.jafc.1c05677.

Cheng, Y.J., Chen, N.N., Li, J., Su, J.C., Yang, J., Zhang, C.X., Lin, H.W., Zhou, Y., 2021. Antimicrobial Chlorinated Carbazole Alkaloids from the Sponge Associated Actinomycete *Streptomyces diacarni* LHW51701. Chin. J. Chem. 39 (5), 1188–1192. https://doi.org/10.1002/cjoc.202000736.

Cockrell, A.L., Fitzgerald, L.A., Cusick, K.D., Barlow, D.E., Tsoi, S. D., Soto, C.M., Baldwin, J.W., Dale, J.R., Morris, R.E., Little, B. J., Biffinger, J.C., 2015. Differences in Physical and Biochemical Properties of *Thermus scotoductus* SA-01 Cultured with Dielectric or Convection Heating. Appl. Environ. Microbiol. 81 (18), 6285–6293. https://doi.org/10.1128/AEM.01618-15.

Côté, H., Pichette, A., Simard, F., Ouellette, M.E., Ripoll, L., Mihoub, M., Grimard, D., Legault, J., 2019. Balsacone C, a New Antibiotic Targeting Bacterial Cell Membranes, Inhibits Clinical Isolates of Methicillin-Resistant *Staphylococcus aureus* (MRSA) Without Inducing Resistance. Front. Microbiol. 10, 2341. https://doi.org/10.3389/fmicb.2019.02341.

DuBois, M., Gilles, K.A., Hamilton, J.K., Rebers, P.A., Smith, F., 2002. Colorimetric Method for Determination of Sugars and Related Substances. Anal. Chem. 28 (3), 350–356. https://doi.org/10.1021/ac60111a017.

Feng, S.M., Liu, Y.J., Li, Q.H., Gui, Z.S., Feng, G.Q., 2022a. Two Water-Soluble and Wash-Free Fluorogenic Probes for Specific Lighting Up Cancer Cell Membranes and Tumors. Anal. Chem. 94 (3), 1601–1607. https://doi.org/10.1021/acs.analchem.1c03685.

Feng, Y.M., Qi, P.Y., Xiao, W.L., Zhang, T.H., Zhou, X., Liu, L.W., Yang, S., 2022b. Fabrication of Isopropanolamine-Decorated Coumarin Derivatives as Novel Quorum Sensing Inhibitors to Suppress Plant Bacterial Disease. J. Agric. Food Chem. 70 (20), 6037–6049. https://doi.org/10.1021/acs.jafc.2c01141.

Fu, B., Dong, X.Y., Yu, X.X., Zhang, Z., Sun, L., Zhu, W.H., Liang, X., Xu, H.J., 2021. *meso*-borneol- and *meso*-carbazole-substituted porphyrins: multifunctional chromophores with tunable electronic structures and antitumor activities. New J. Chem. 45 (4), 2141–2146. https://doi.org/10.1039/D0NJ02954H.

Gan, B.H., Cai, X., Javor, S., Kohler, T., Reymond, J.L., 2020. Synergistic Effect of Propidium Iodide and Small Molecule Antibiotics with the Antimicrobial Peptide Dendrimer G3KL against Gram-Negative Bacteria. Molecules 25 (23), 5643. https://doi.org/10.3390/molecules25235643.

Gao, M.N., Yu, L., Li, P., Song, X.P., Chen, Z., He, M., Song, B.A., 2017. Label-free quantitative proteomic analysis of inhibition of *Xanthomonas axonopodis* pv. *citri* by the novel bactericide Fubianezuofeng. Pestic. Biochem. Phys. 138, 37–42. https://doi.org/10.1016/j.pestbp.2017.02.004.

Grau, L., Romero, M., Privat-Contreras, C., Presa, D., Vinas, M., Morral, J., Pors, K., Rubio-Martinez, J., Pujol, M.D., 2020. Multigram scale synthesis of polycyclic lactones and evaluation of antitumor and other biological properties. Eur. J. Med. Chem. 185,. https://doi.org/10.1016/j.ejmech.2019.111807 111807.

He, Q., Zhang, L.J., Song, L.Y., Zhang, X.H., Liu, D.H., Hu, Y.Q., Guo, M.M., 2021. Inactivation of Staphylococcus aureus using ultrasound in combination with thyme essential oil nanoemulsions and its synergistic mechanism. LWT-Food Sci. Technol. 147,. https://doi.org/10.1016/j.lwt.2021.111574 111574.

Huang, X., Liu, H.W., Long, Z.Q., Li, Z.X., Zhu, J.J., Wang, P.Y., Qi, P.Y., Liu, L.W., Yang, S., 2021. Rational Optimization of 1,2,3-Triazole-Tailored Carbazoles As Prospective Antibacterial Alternatives with Significant In Vivo Control Efficiency and Unique Mode of Action. J. Agric. Food Chem. 69 (16), 4615–4627. https://doi.org/10.1021/acs.jafc.1c00707.

Hurley, K.A., Heinrich, V.A., Hershfield, J.R., Demons, S.T., Weibel, D.B., 2015. Membrane-Targeting DCAP Analogues with Broad-Spectrum Antibiotic Activity against Pathogenic Bacteria. ACS Med. Chem. Lett. 6 (4), 466–471. https://doi.org/10.1021/acsmedchemlett.5b00024.

Li, P., Tian, P.Y., Chen, Y.Z., Song, X.P., Xue, W., Jin, L.H., Hu, D. Y., Yang, S., Song, B.A., 2018. Novel bisthioether derivatives containing a 1,3,4-oxadiazole moiety: design, synthesis, antibacterial and nematocidal activities. Pest Manag. Sci. 74 (4), 844–852. https://doi.org/10.1002/ps.4762.

Lin, S.M., Liu, J.Y., Li, H.X., Liu, Y., Chen, Y.Z., Luo, J.C., Liu, S. P., 2020. Development of Highly Potent Carbazole Amphiphiles as Membrane-Targeting Antimicrobials for Treating Gram-Positive Bacterial Infections. J. Med. Chem. 63 (17), 9284–9299. https://doi.org/10.1021/acs.jmedchem.0c00433.

Liu, W., Zhao, C., Liu, L., Huang, D., Ma, C., Li, R., Huang, L.L., 2022. Genome-wide identification of the TGA gene family in kiwifruit (*Actinidia chinensis* spp.) and revealing its roles in response to *Pseudomonas syringae* pv. *actinidiae* (*Psa*) infection. Int. J. Biol. Macromol. 222 (Part A), 101-113. https://doi.org/10.1016/j.ijbiomac.2022.09.154.

Liu, D.Y., Song, R.J., Wu, Z.X., Xing, Z.F., Hu, D.Y., 2022b. Pyrido [1,2-*a*] Pyrimidinone Mesoionic Compounds Containing Vanillin Moiety: Design, Synthesis, Antibacterial Activity, and Mechanism. J. Agric. Food Chem. 70 (34), 10443–10452. https://doi.org/10.1021/acs.jafc.2c01838.

Moon, H., Jeong, A.R., Kwon, O.K., Park, C.J., 2022. *Oryza*-Specific Orphan Protein Triggers Enhanced Resistance to *Xanthomonas oryzae* pv. *oryzae* in Rice. Front. Plant Sci. 13,. https://doi.org/10.3389/fpls.2022.859375 859375.

Mukhtar, A., Manzoor, M., Gul, I., Zafar, R., Jamil, H.I., Niazi, A. K., Ali, M.A., Park, T.J., Arshad, M., 2020. Phytotoxicity of different antibiotics to rice and stress alleviation upon application of organic amendments. Chemosphere 258,. https://doi.org/10.1016/j.chemosphere.2020.127353 127353.

Nalli, Y., Khajuria, V., Gupta, S., Arora, P., Riyaz-Ul-Hassan, S., Ahmed, Z., Ali, A., 2016. Four new carbazole alkaloids from *Murraya koenigii* that display anti-inflammatory and anti-microbial activities. Org. Biomol. Chem. 14 (12), 3322–3332. https://doi.org/10.1039/C6OB00267F.

Nayem, S.A., Chowdhury, M.S.M., Sultana, N., Masum, G.Z.H., Rahman, M.S., Jamal, M.A.H.M., 2020. Combined effect of salt stress and *Xanthomonas axonopodis* pv *citri* on citrus (*Citrus aurantifolia*). Heliyon 6 (2), e03403.

Ning, H.Q., Li, Y.Q., Tian, Q.W., Wang, Z.S., Mo, H.Z., 2019. The apoptosis of *Staphylococcus aureus* induced by glycinin basic peptide through ROS oxidative stress response. LWT-Food Sci. Technol. 99, 62–68. https://doi.org/10.1016/j.lwt.2018.09.028.

Ojeda, J.J., Romero-González, M.E., Bachmann, R.T., Edyvean, R.G. J., Banwart, S.A., 2008. Characterization of the cell surface and cell wall chemistry of drinking water bacteria by combining XPS, FTIR spectroscopy, modeling, and potentiometric titrations. Langmuir. 24, 4032–4040. https://doi.org/10.1021/la702284b.

Parra, A., Clares, B., Rossello, A., Garduno-Ramirez, M.L., Abrego, G., Garcia, M.L., Calpena, A.C., 2016. Ex vivo permeation of carprofen from nanoparticles: A comprehensive study through human, porcine and bovine skin as anti-inflammatory agent. Int. J. Pharm. 501, 10–17. https://doi.org/10.1016/j.ijpharm.2016.01.056.

Pattanashetty, S.H., Hosamani, K.M., Shettar, A.K., Mohammed, S. R., 2018. Design, Synthesis and Computational Studies of Novel Carbazole *N*-phenylacetamide Hybrids as Potent Antibacterial, Anti-inflammatory, and Antioxidant Agents. J. Heterocyclic Chem. 55 (7), 1765–1774. https://doi.org/10.1002/jhet.3214.

Pereira, A.D.E.S., Luiz de Oliveira, J., Maira Savassa, S., Barbara Rogério, C., Araujo de Medeiros, G., Fraceto, L.F., 2022. Lignin nanoparticles: New insights for a sustainable agriculture. J. Clean. Prod. 345,. https://doi.org/10.1016/j.jclepro.2022.131145 131145.

Picchi, S.C., Granato, L.M., Franzini, M.J.F., Andrade, M.O., Takita, M.A., Machado, M.A., Souza, A.A.D., 2021. Modified Monosaccharides Content of *Xanthan* Gum Impairs Citrus Canker Disease by Affecting the Epiphytic Lifestyle of *Xanthomonas citri* subsp. *citri*. Microorganisms 9 (6), 1176. https://doi.org/10.3390/microorganisms9061176.

Poonprasartporn, A., Chan, K.L.A., 2021. Live-cell ATR-FTIR spectroscopy as a novel bioanalytical tool for cell glucose metabolism research. BBA Mol. Cell Res. 1868, (7). https://doi.org/10.1016/j.bbamcr.2021.119024 119024.

Prasad, H.S.N., Ananda, A.P., Lohith, T.N., Prabhuprasad, P., Jayanth, H.S., Krishnamurthy, N.B., Sridhar, M.A., Mallesha, L., Mallu, P., 2022. Design, synthesis, molecular docking and DFT computational insight on the structure of Piperazine sulfynol derivatives as a new antibacterial contender against superbugs MRSA. J. Mol. Struct. 1247,. https://doi.org/10.1016/j.molstruc.2021.131333 131333.

Qi, P.Y., Zhang, T.H., Feng, Y.M., Wang, M.W., Shao, W.B., Zeng, D., Jin, L.H., Wang, P.Y., Zhou, X., Yang, S., 2022. Exploring an Innovative Strategy for Suppressing Bacterial Plant Disease: Excavated Novel Isopropanolamine-Tailored Pterostilbene Derivatives as Potential Antibiofilm Agents. J. Agric. Food Chem. 70 (16), 4899–4911. https://doi.org/10.1021/acs.jafc.2c00590.

Salih, N., Salimon, J., Yousif, E., 2016. Synthesis and antimicrobial activities of 9*H*-carbazole derivatives. Arab. J. Chem. 9, S781–S786. https://doi.org/10.1016/j.arabjc.2011.08.013.

Sciallano, C., Auguy, F., Boulard, G., Szurek, B., Cunnac, S., 2022. The Complete Genome Resource of *Xanthomonas oryzae* pv. *oryzae* CIX2779 Includes the First Sequence of a Plasmid for an African Representative of This Rice Pathogen. Mol. Plant-Microbe Interact. 36 (1), 73–77. https://doi.org/10.1094/MPMI-09-22-0191-A.

Song, Y.L., Liu, S.S., Yang, J., Xie, J., Zhou, X., Wu, Z.B., Liu, L.W., Wang, P.Y., Yang, S., 2022. Discovery of Epipodophyllotoxin-Derived B_2 as Promising *Xoo*FtsZ Inhibitor for Controlling Bacterial Cell Division: Structure-Based Virtual Screening, Synthesis, and SAR Study. Int. J. Mol. Sci. 23 (16), 9119. https://doi.org/10.3390/ijms23169119.

Stenclova, P., Freisinger, S., Barth, H., Kromka, A., Mizaikoff, B., 2019. Cyclic Changes in the Amide Bands Within *Escherichia coli* Biofilms Monitored Using Real-Time Infrared Attenuated Total Reflection Spectroscopy (IR-ATR). Appl Spectrosc. 73, 424–432. https://doi.org/10.1177/0003702819829081.

Sutherland, I.W., 1982. Biosynthesis of microbial exopolysaccharides. Adv. Microb. Physiol. 23, 79–150. https://doi.org/10.1016/S0065-2911(08)60336-7.

Tahir, J., Brendolise, C., Hoyte, S., Lucas, M., Thomson, S., Hoeata, K., McKenzie, C., Wotton, A., Funnell, K., Morgan, E., Hedderley, D., Chagne, D., Bourke, P.M., McCallum, J., Gardiner, S.E., Gea, L., 2020. QTL Mapping for Resistance to Cankers Induced by *Pseudomonas syringae* pv. *actinidiae* (Psa) in a Tetraploid *Actinidia chinensis* Kiwifruit Population. Pathogens 9 (11), 967 https://www.mdpi.com/2076-0817/9/11/967.

Thawabteh, A., Juma, S., Bader, M., Karaman, D., Scrano, L., Bufo, S.A., Karaman, R., 2019. The Biological Activity of Natural Alkaloids against Herbivores. Cancerous Cells and Pathogens. Toxins 11 (11), 656. https://doi.org/10.3390/toxins11110656.

Wang, F., Liu, H.W., Zhang, L., Liu, S.T., Zhang, J.R., Zhou, X., Wang, P.Y., Yang, S., 2022. Discovery of novel rost-4-ene derivatives as potential plant activators for preventing phytopathogenic bacterial infection: Design, synthesis and biological studies. Pest Manag. Sci. 78 (8), 3404–3415. https://doi.org/10.1002/ps.6981.

Wang, F., Yang, B.X., Zhang, T.H., Tao, Q.Q., Zhou, X., Wang, P.Y., Yang, S., 2023. Novel 1,3,4-oxadiazole thioether and sulfone derivatives bearing a flexible *N*-heterocyclic moiety: Synthesis, characterization, and anti-microorganism activity. Arab. J. Chem. 16, (2). https://doi.org/10.1016/j.arabjc.2022.104479 104479.

Wicaksono, W.A., Jones, E.E., Casonato, S., Monk, J., Ridgway, H.J., 2018. Biological control of *Pseudomonas syringae* pv. *actinidiae* (*Psa*), the causal agent of bacterial canker of kiwifruit, using endophytic bacteria recovered from a medicinal plant. Biol. Control. 116, 103–112. https://doi.org/10.1016/j.biocontrol.2017.03.003.

Xiang, Q., Kang, C.D., Niu, L.Y., Zhao, D.B., Li, K., Bai, Y.H., 2018. Antibacterial activity and a membrane damage mechanism of plasma-activated water against *Pseudomonas deceptionensis* CM2. LWT-Food Sci. Technol. 96, 395–401. https://doi.org/10.1016/j.lwt.2018.05.059.

Xiong, G., Wu, Z., Yi, J., Fu, L., Yang, Z., Hsieh, C., Yin, M., Zeng, X., Wu, C., Lu, A., Chen, X., Hou, T., Cao, D., 2021. ADMETlab 2.0: an integrated online platform for accurate and comprehensive predictions of ADMET properties. Nucleic Acids Res. 49 (W1), W5–W14. https://doi.org/10.1093/nar/gkab255.

Xue, Y.J., Li, M.Y., Jin, X.J., Zheng, C.J., Piao, H.R., 2021. Design, synthesis and evaluation of carbazole derivatives as potential antimicrobial agents. J. Enzyme. Inhib. Med. Chem. 36 (1), 295–306. https://doi.org/10.1080/14756366.2020.1850713.

Yang, T., Zhang, T., Zhou, X., Wang, P.Y., Gan, J.H., Song, B.A., Yang, S., Yang, C.G., 2021. Dysregulation of ClpP by Small-Molecule Activators Used Against *Xanthomonas oryzae* pv. *oryzae* Infections. J. Agric. Food Chem. 69 (27), 7545–7553. https://doi.org/10.1021/acs.jafc.1c01470.

Zang, H.J., Qian, G.Q., Arbiser, J., Owonikoko, T.K., Ramalingam, S.S., Fan, S.Q., Sun, S.Y., 2020. Overcoming acquired resistance of EGFR-mutant NSCLC cells to the third generation EGFR inhibitor, osimertinib, with the natural product honokiol. Mol. Oncol. 14 (4), 882–895. https://doi.org/10.1002/1878-0261.12645.

Zeng, L., Xu, J.F., Zhang, X., 2022. Degradable Bactericide Constructed Using a Charge-Reversal Surfactant against Plant Pathogenic Bacteria. ACS Appl. Mater. Interfaces 14 (8), 10134–10141. https://doi.org/10.1021/acsami.1c24588.

Zhang, N., Fan, Y.X., Li, C., Wang, Q.M., Leksawasdi, N., Li, F.L., Wang, S.A., 2018. Cell permeability and nuclear DNA staining by propidium iodide in basidiomycetous yeasts. Appl. Microbiol. Biotechnol. 102 (9), 4183–4191. https://doi.org/10.1007/s00253-018-8906-8.

Zhang, F.F., Gan, L.L., Zhou, C.H., 2010. Synthesis, antibacterial and antifungal activities of some carbazole derivatives. Bioorg. Med. Chem. Lett. 20 (6), 1881–1884. https://doi.org/10.1016/j.bmcl.2010.01.159.

Zhao, Y.L., Huang, X., Liu, L.W., Wang, P.Y., Long, Q.S., Tao, Q. Q., Li, Z., Yang, S., 2019. Identification of Racemic and Chiral Carbazole Derivatives Containing an Isopropanolamine Linker as Prospective Surrogates against Plant Pathogenic Bacteria: *In Vitro* and *In Vivo* Assays and Quantitative Proteomics. J. Agric. Food Chem. 67 (26), 7512–7525. https://doi.org/10.1021/acs.jafc.9b02036.

Zheng, D.H., Wang, H.H., Zhong, H., Ke, W.L., Hu, H.F., Sun, M., Ruan, L.F., 2021. Elucidation of the Pathogenicity-Associated Regulatory Network in *Xanthomonas oryzae* pv. *oryzae*. mSystems 6 (2), e00789–e820. https://doi.org/10.1128/mSystems.00789-20.

Zhou, X., Ye, H.J., Gao, X.H., Feng, Y.M., Shao, W.B., Qi, P.Y., Wu, Z.B., Liu, L.W., Wang, P.Y., Yang, S., 2021. The discovery of natural 4'-demethylepipodophyllotoxin from renewable *Dysosma versipellis* species as a novel bacterial cell division inhibitor for

controlling intractable diseases in rice. Ind. Crop. Prod. 174,. https://doi.org/10.1016/j.indcrop.2021.114182 114182.

Zhou, X., Fu, Y.H., Zou, Y.Y., Meng, J., Ou-Yang, G.P., Ge, Q.S., Wang, Z.C., 2022b. Discovery of Simple Diacylhydrazine-Functionalized Cinnamic Acid Derivatives as Potential Microtubule Stabilizers. Int. J. Mol. Sci. 23 (20), 12365. https://doi.org/10.3390/ijms232012365.

Zhou, Q., Li, L.W., Liu, F., Hu, J., Cao, Y., Qiao, S.W., Zhou, Y.X., Wang, B., Jia, Y.H., Chen, Y., Xu, S., Feng, X., 2022a. Mining and characterization of oxidative stress-related binding proteins of parthenolide in *Xanthomonas oryzae* pv. *oryzae*. Pest Manag. Sci. 78 (8), 3345–3355. https://doi.org/10.1002/ps.6961.

Zhu, D.Q., Chen, M.H., Li, M., Luo, B.L., Zhao, Y., Huang, P., Xue, F.T., Rapposelli, S., Pi, R.B., Wen, S., 2013. Discovery of novel *N*-substituted carbazoles as neuroprotective agents with potent antioxidative activity. Eur. J. Med. Chem. 68, 81–88. https://doi.org/10.1016/j.ejmech.2013.07.029.

Zhu, M., Li, Y., Long, X.S., Wang, C.Y., Ouyang, G.P., Wang, Z.C., 2022. Antibacterial Activity of Allicin-Inspired Disulfide Derivatives against *Xanthomonas axonopodis* pv. *citri*. Int. J. Mol. Sci. 23 (19), 11947. https://doi.org/10.3390/ijms231911947.